Modular Flows: Differential Molecular Generation

Anonymous Author(s)
Affiliation
Address
email

Abstract

Generating new molecules is fundamental to advancing critical applications such as drug discovery and material synthesis. Flows can generate molecules effectively by inverting the encoding process, however, existing flow models either require artifactual dequantization or specific node/edge orderings, lack desiderata such as permutation invariance, or induce discrepancy between encoding and decoding steps that necessitates *post hoc* validity correction. We circumvent these issues with novel continuous normalizing E(3)-equivariant flows, based on a system of node ODEs coupled as a graph PDE, that repeatedly reconcile locally toward globally aligned densities. Our models can be cast as message passing temporal networks, and result in superlative performance on the tasks of density estimation and molecular generation. In particular, our generated samples achieve state of the art on both the standard QM9 and ZINC250K benchmarks.

1 Introduction

Generative models have rapidly become ubiquitous in machine learning with advances from image synthesis (Ramesh et al., 2022) to protein design (Ingraham et al., 2019). Molecular generation (Stokes et al., 2020) has also received significant attention owing to its promise for discovering new drugs and materials. Searching for valid molecules in prohibitively large discrete spaces is, however, challenging: estimates for drug-like structures range between 10^{23} and 10^{60} but only a tiny fraction - on the order of 10^8 - has been synthesized (Polishchuk et al., 2013; Merz et al., 2020). Thus, learning representations that exploit appropriate molecular inductive biases (e.g., spatial correlations) becomes crucial.

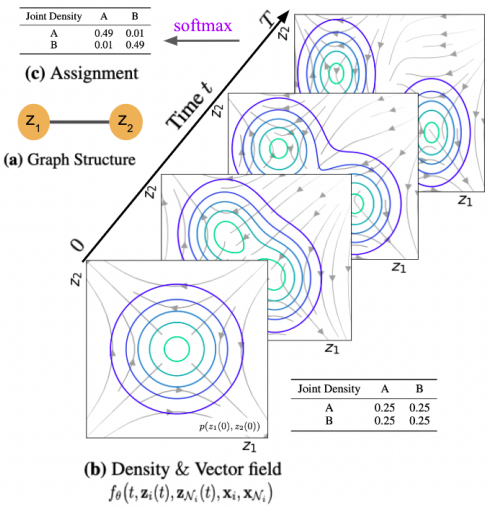

Figure 1: A toy illustration of `ModFlow` in action with a two-node graph. The two local flows - $\mathbf{z}_1$ and $\mathbf{z}_2$ - co-evolve toward a more complex joint density, both driven by the same differential f.

Earlier models focused on generating sequences based on the SMILES notation (Weininger, 1988) used in Chemistry to describe the molecular structure as strings. However, they were supplanted by generative models that capture valuable spatial information such as bond strengths and dihedral angles, e.g., by embedding molecular graphs via some graph neural network (GNNs) (Scarselli et al., 2009; Garg et al., 2020). Such models primarily include variants of Generative Adversarial Networks (GANs), Variational Autoencoders (VAEs), and Normalizing Flows

Submitted to 36th Conference on Neural Information Processing Systems (NeurIPS 2022). Do not distribute.

(Dinh et al., 2014, 2016). Besides known issues with training, GANs (Goodfellow et al., 2014; Maziarka et al., 2020) suffer from the well-documented problem of mode collapse, thereby generating molecules that lack diversity. VAEs (Kingma and Welling, 2013; Lim et al., 2018; Jin et al., 2018), on the other hand, are susceptible to a distributional shift between the training data and the generated samples. Moreover, optimizing for likelihood via a surrogate lower bound is likely insufficient to capture the complex dependencies inherent in molecules.

Flows are especially appealing since, in principle, they enable estimating (and sampling from) complex data distributions using a sequence of invertible transformations on samples from a more tractable continuous distribution. Molecules are discrete, so many flow models (Madhawa et al., 2019; Honda et al., 2019; Shi et al., 2020) add noise during encoding and later apply a *dequantization* procedure. However, dequantization begets distortion and issues related to convergence (Luo et al., 2021). Moroever, many methods segregate the generation of atoms from bonds, so the assembled structure is often not a valid molecule and requires *post hoc* correction to ensure validity (Zang and Wang, 2020), effecting a discrepancy between the encoding and the decoded distributions. Permutation dependence is another undesirable artifact of these methods. Some alternatives have been explored to avoid dequantization, e.g., (Lippe and Gavves, 2021) encodes molecules in a continuous latent space via variational inference and jointly optimizes a flow model for generation. Discrete graph flows (Luo et al., 2021) also circumvent the many pitfalls of dequantization by resorting to discrete latent variables, and performing validity checks during the generative process. However, discrete flows follow an autoregressive procedure that requires a specific ordering of nodes and edges during training. In general, one shot methods can generate much faster than discrete flows.

We offer a different flow-based perspective tailored to molecules. Specifically, we suggest coupled continuous normalizing E(3)-equivariant flows that bestow generative capabilities from neural partial differential equation (PDE) models on graphs. Graph PDEs have been known to enable designing new embedding methods such as variants of GNNs (Chamberlain et al., 2021), extending GNNs to continuous layers as Neural ODEs (Poli et al., 2019), and accommodating spatial information (Iakovlev et al., 2020). We instead seek to bring to the fore their efficacy and elegance as tools to help generate complex objects, such as molecules, viewed as outcomes resulting from an interplay of co-adapting latent trajectories (i.e., underlying dynamics). Concretely, a flow is associated with each node of the graph, and these flows are conjoined as a joint ODE system conditioned on neighboring nodes. While these flows originate independently as samples from simple distributions, they adjust progressively toward more complex joint distributions as they repeatedly interact with the neighboring flows. We view molecules as samples generated from the globally aligned distributions obtained after many such local feedback iterations. We call the proposed method Modular Flows (`ModFlow`) to underscore that each node can be regarded as a module that coordinates with other modules. Table 1 summarizes the capabilities of `ModFlow` compared to some previous generative works.

Contributions. We propose to learn continuous-time, flow based generative models, grounded on graph PDEs, for generating molecules without any validity correction. In particular,

Table 1: A comparison of generative modeling approaches for molecules.

Method	One-shot	Modular	Invertible	Continuous-time	
JT-VAE	✓	✓	✗	✗	Jin et al. (2018)
MRNN	✗	✗	✗	✗	Popova et al. (2019)
GraphAF	✗	✗	✓	✗	Shi et al. (2020)
GraphDF	✗	✗	✓	✗	Luo et al. (2021)
MoFlow	✓	✗	✓	✗	Zang and Wang (2020)
GraphNVP	✓	✗	✓	✗	Madhawa et al. (2019)
`ModFlow`	✓	✓	✓	✓	this work

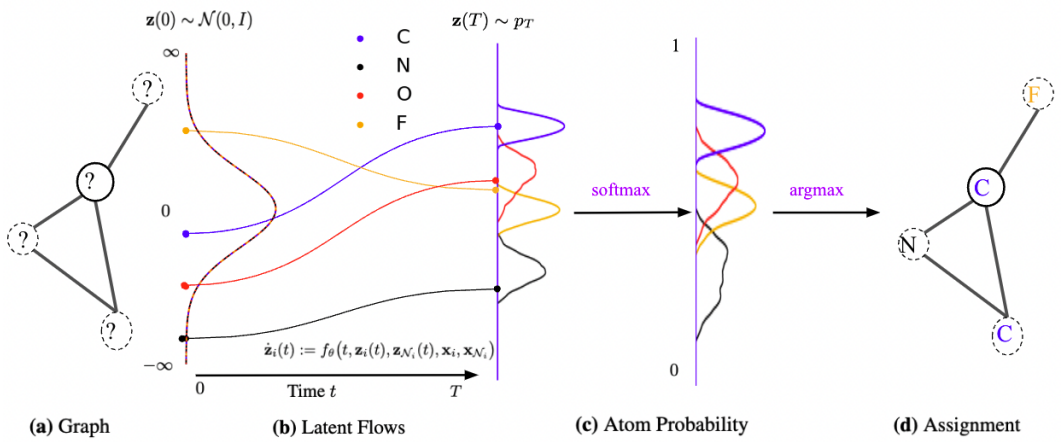

Figure 2: A demonstration of the modular flow generation. The initial Gaussian distributions $\mathcal{N}(0, I)$ evolve into complex densities $\mathbf{z}(T)$ by the flow f and are subsequently turned to probabilities and labels.

- we propose `ModFlow`, a novel generative model based on coupled continuous normalizing E(3)-equivariant flows. `ModFlow` encapsulates essential inductive bias using PDEs, and defines multiple flows that interact locally toward a globally consistent joint density;
- we encode permutation, translation, rotation, and reflection equivariance, with E(3) equivariant GNNs adapted to molecular generation, and can leverage 3D geometric information;
- `ModFlow` is end-to-end trainable, non-autoregressive, and obviates the need for any external validity checks or correction;
- empirically, `ModFlow` achieves state-of-the-art performance on both the standard QM9 (Ramakrishnan et al., 2014) and ZINC250K (Irwin et al., 2012) benchmarks.

2 Related works

Generative models. Earlier attempts for molecule generation (Kusner et al., 2017; Dai et al., 2018) aimed at representing molecules as SMILES strings (Weininger, 1988) and developed sequence generation models. One of the challenges of these approaches is to learn complicated grammar rules that can generate syntactically valid sequences of molecules. Recently, representing molecules as graphs has inspired new deep generative model for molecular generation (Segler et al., 2018; Samanta et al., 2018; Neil et al., 2018) ranging from VAEs (Jin et al., 2018; Kajino, 2019) to flows (Madhawa et al., 2019; Luo et al., 2021; Shi et al., 2020). The core idea is to learn to encode molecular graphs into a latent space, and subsequently decode samples from the latent space to generate new molecules (Atwood and Towsley, 2016; Xhonneux et al., 2020; You et al., 2018).

Graph partial differential equations. Graph PDEs is an emerging area that studies PDEs on structured data encoded as graphs. For instance, one can define a PDE on graphs to track the evolution of signals defined over the graph nodes under some dynamics. Graph PDEs have enabled, among others, design of new graph neural networks; see, e.g., works such as GRAND (Chamberlain et al., 2021), GNODE (Poli et al., 2019), NeuralPDE (Iakovlev et al., 2020), Neural operator (Li et al., 2020) and PDE-GCN (Eliasof et al., 2021). Different from all these works, we focus on using PDEs for generative modeling of molecules (graph-structured objects). Interestingly, `ModFlow` proposed in this work may be viewed as a new equivariant temporal graph network.

Validity oracles. A key challenge of molecular generative models is to be able to generate valid molecules, according to various criteria for molecular validity or feasibility. It is a common practice to use external chemical software as rejection oracles to reduce or exclude invalid molecules, or do

validity checks as part of autoregressive generation. (Luo et al., 2021; Shi et al., 2020; Popova et al., 2019). An important open question has been whether generative models can learn to achieve high generative validity *intrinsically*, i.e., without being aided by oracles or performing additional checks. `ModFlow` represents a major step forward toward that goal.

3 Modular Flows

We focus on unsupervised learning of an underlying graph density $p(G)$ using a dataset $\mathcal{D} = \{G_n\}_{n=1}^N$ of observed molecular graphs G_n. We learn a generative flow model $p_\theta(G)$ specified by flow parameters θ, and use it to sample novel high-probability molecules.

3.1 Molecular Representation

Graph representation. We represent the molecular graph $G = (V, E)$ of size M as a tuple of vertices $V = (v_1, \ldots, v_M)$ and edges $E \subset V \times V$. Each vertex takes value from an alphabet on atoms: $v \in \mathcal{A} = \{\mathtt{C}, \mathtt{H}, \mathtt{N}, \mathtt{O}, \mathtt{P}, \mathtt{S}, \ldots\}$; while the edges $e \in \mathcal{B} = \{1, 2, 3\}$ abstract the type of bond (i.e., single, double, or triple). We assume that, conditioned on the edges, the graph likelihood factorizes as a Categorical distribution over vertices given their latent representations:

$$p(G) := p(V|E, \{z\}) = \prod_{i=1}^{M} \mathrm{Cat}(v_i|\sigma(\mathbf{z}_i)), \tag{1}$$

where $\mathbf{z}_i = (z_{i\mathtt{C}}, z_{i\mathtt{H}}, \ldots) \in \mathbb{R}^{|\mathcal{A}|}$ is a set of atom score parameters, where $z_{ik} \in \mathbb{R}$ pertains to node i and type $k \in \mathcal{A}$, and σ is the softmax function

$$\sigma(\mathbf{z}_i)_k = \frac{\exp \mathbf{z}_{ik}}{\sum_{k'} \exp \mathbf{z}_{ik'}}\ , \tag{2}$$

which turns the real-valued scores $\mathbf{z}_i$ of a node i into normalized probabilities. `ModFlow` also supports 3D molecular graphs that contain atomic coordinates and angles.

Tree representations. We can obtain an alternative representation for molecules based on decomposing a molecule into a tree-like structure, by contracting certain vertices into a single node (denoted as a cluster) such that the molecular graph G becomes acyclic. Following the decomposition investigated by Jin et al. (2018), we restrict these clusters to ring-substructures present in the molecular data, in addition to the atom alphabet. Thus, we obtain an extended alphabet $\mathcal{A}_{\mathrm{tree}} = \{\mathtt{C}, \mathtt{H}, \mathtt{N}, \ldots, \mathtt{C}_1, \mathtt{C}_2, \ldots\}$, where each cluster label $\mathtt{C}_r$ corresponds to the some ring-substructure in the label vocabulary χ. We reduce the vocabulary to the 30 most commonly occurring substructures of $\mathcal{A}_{\mathrm{tree}}$. For further details, see Appendix A.1.

3.2 Differential modular flows

Normalizing flows (Kobyzev et al., 2021) provide a general recipe for constructing flexible probability distributions, used in density estimation (Cramer et al., 2021; Huang et al., 2018) and generative modeling (Zhen et al., 2020; Zang and Wang, 2020). We propose to model the atom scores $\mathbf{z}_i(t)$ as a Continuous-time Normalizing Flow (CNF) (Grathwohl et al., 2018) over time $t \in \mathbb{R}_+$. We assume the initial scores at time $t = 0$ follow an uninformative Gaussian base distribution $\mathbf{z}_i(0) \sim \mathcal{N}(0, I)$ for each node i. Node scores evolve in parallel over time by a differential equation,

$$\dot{\mathbf{z}}_i(t) := \frac{\partial \mathbf{z}_i(t)}{\partial t} = f_\theta\big(t, \mathbf{z}_i(t), \mathbf{z}_{\mathcal{N}_i}(t), \mathbf{x}_i, \mathbf{x}_{\mathcal{N}_i}\big), \qquad i = 1, \ldots, M \tag{3}$$

where $\mathcal{N}_i = \{\mathbf{z}_j : (i, j) \in E\}$ is the set of neighbor scores at time t, $\mathbf{x}_i, \mathbf{x}_{\mathcal{N}_i}$ is the positional information (2D/3D) of node and the neighbours, and θ are the parameters of the flow function f to be learned. By collecting all node differentials we obtain a *modular* joint, coupled ODE, which is our

key contribution:,

$$\dot{\mathbf{z}}(t) = \begin{pmatrix} \dot{\mathbf{z}}_1(t) \\ \vdots \\ \dot{\mathbf{z}}_M(t) \end{pmatrix} = \begin{pmatrix} f_\theta\big(t, \mathbf{z}_1(t), \mathbf{z}_{\mathcal{N}_1}(t), \mathbf{x}_i, \mathbf{x}_{\mathcal{N}_i}\big) \\ \vdots \\ f_\theta\big(t, \mathbf{z}_M(t), \mathbf{z}_{\mathcal{N}_M}(t), \mathbf{x}_i, \mathbf{x}_{\mathcal{N}_i}\big) \end{pmatrix} \tag{4}$$

$$\mathbf{z}(T) = \mathbf{z}(0) + \int_0^T \dot{\mathbf{z}}(t)dt. \tag{5}$$

The coupled system of ODEs is equivalent to a graph PDE (Iakovlev et al., 2020; Chamberlain et al., 2021), where the evolution of each node only depends on its immediate neighbors.

The flow induces corresponding density changes by the divergence of f, (Chen et al., 2018)

$$\frac{d \log p_t(\mathbf{z}_i(t))}{dt} = -\operatorname{tr}\left(\frac{\partial f_\theta\big(t, \mathbf{z}_i(t), \mathbf{z}_{\mathcal{N}_i}(t), \mathbf{x}_i, \mathbf{x}_{\mathcal{N}_i}\big)}{\partial \mathbf{z}_i}\right), \tag{6}$$

starting from the base distribution $p_0(\mathbf{z}_i(0)) = \mathcal{N}(\mathbf{z}_i(0)|0, I)$. The trace picks only the diagonal elements of the Jacobian $\frac{\partial f}{\partial \mathbf{z}}$, which interprets the neighborhood input $\mathbf{z}_{\mathcal{N}_i}$ term as a 'control' for each node $\mathbf{z}_i$ at each instant t. The above system is usually solved via an ODE solver where gradients are computed via adjoint sensitivity method (Kolmogorov et al., 1962). This approach incurs a low memory cost, and explicitly controls numerical error. Notably, moving towards modular flows translates sparsity also to the adjoints.

Preposition 1: *Modular adjoints are sparser than regular adjoints. They can be computed by*

$$\frac{d\boldsymbol{\lambda}_i}{dt} = -\boldsymbol{\lambda}(t)^\top \frac{\partial f\big(t, \mathbf{z}_i(t), \mathbf{z}_{\mathcal{N}_i}(t), \mathbf{x}_i, \mathbf{x}_{\mathcal{N}_i}\big)}{\partial \mathbf{z}} = -\sum_{j \in \mathcal{N}_i \cup \{i\}} \boldsymbol{\lambda}_j(t)^\top \frac{\partial f\big(t, \mathbf{z}_i(t), \mathbf{z}_{\mathcal{N}_i}(t), \mathbf{x}_i, \mathbf{x}_{\mathcal{N}_i}\big)}{\partial \mathbf{z}_j}, \tag{7}$$

where the partial derivatives $\frac{\partial f}{\partial \mathbf{z}} = [\frac{\partial f_i}{\partial \mathbf{z}_j}]_{ij}$ *are sparse* (See Appendix A.5 for derivation).

3.3 Equivariant local differential

Our goal is to have a differential function f that is a PDE operator used in Eq. 4, and that satisfies the natural equivariances and invariances of molecules. Specifically, the function must be (i) translation equivariant: translating the input results in an equivalent translation of the output; (ii) rotational (and reflection) equivariant: rotating the input results in an equivalent rotation of the output; (iii) permutation equivariant: permuting the input results in the same permutation of the output. Therefore, we chose to use E(3)-Equivariant GNN (EGNN) (Satorras et al., 2021), which is translation, rotation and reflection equivariant (E(n)), and permutation equivariant with respect to an input set of points (See Appendix A.2 for details). The input to the EGNN are the node embeddings and the geometric information (polar coordinates (2D) and spherical polar coordinates (3D)). Interestingly, `ModFlow` can be viewed as a message passing temporal graph network (Rossi et al., 2020) as shown next.

Preposition 2: *Modular Flows can be cast as Temporal Graph Networks (TGN). The operations are listed in Table 2, where* `ModFlow` *is subjected to a single layer of EGNN.* (See Appendix A.3 for more details).

3.4 Training objective

Normalizing flows are predominantly trained to minimize KL divergence $\mathrm{KL}[p_{\mathrm{data}}||p_\theta]$ between the unknown data distribution p and the flow-generated distribution p_θ. This is equivalent to maximizing their cross-entropy $\mathbb{E}_{p_{\mathrm{data}}}[\log p_\theta]$ (Papamakarios et al., 2021). However, this requires the observations to live in the flow space, which is not true for us: the discrete graphs G and continuous atom scores $\mathbf{z}(t)$ reside in different spaces. To apply normalizing flows, a mapping between the spaces is needed.

Table 2: `ModFlow` as temporal graph networks. We use the shorthand $\mathbf{r}_{ij} = (\mathbf{x}_i - \mathbf{x}_j)$, a_{ij} denote the attributes of the edge between nodes i and j, $\mathbf{s}_i$ is memory state of node (TGN), and $\mathbf{v}_i, \mathbf{e}_{ij}$ are, respectively, the node features and the edge features.

Method	TGN layer	`ModFlow`
Edge	$\mathbf{m}_i'(t) = \text{msg}\left(\mathbf{s}_i\left(t^-\right), t, \mathbf{v}_i(t)\right)$ $\overline{\mathbf{m}}_i'(t) = \text{agg}\left(\mathbf{m}_i'\left(t_1\right), \ldots, \mathbf{m}_i'\left(t_b\right)\right)$	$\mathbf{m}_{ij}(t) = \phi_e\left(\mathbf{z}_i(t), \mathbf{z}_j(t), \left\|\mathbf{r}_{ij}(t)\right\|^2, a_{ij}\right)$ $\hat{\mathbf{m}}_{ij}(t) = \mathbf{r}_{ij}(t) \cdot \phi_x\left(\mathbf{m}_{ij}(t)\right)$ $\mathbf{m}_i(t) = \sum_{j \in \mathcal{N}(i)} \mathbf{m}_{ij}$ $\hat{\mathbf{m}}_i(t) = C \cdot \sum_{j \in \mathcal{N}(i)} \hat{\mathbf{m}}_{ij}(t)$
Memory state	$\mathbf{s}_i(t) = \text{mem}\left(\overline{\mathbf{m}}_i'(t), \mathbf{s}_i\left(t^-\right)\right)$	$\mathbf{x}_i(t+1) = \mathbf{x}_i(t) + \hat{\mathbf{m}}_i(t)$
Node	$\mathbf{z}_i'(t) = \sum_{j \in n_i^k([0,t])} h\left(\mathbf{s}_i(t), \mathbf{s}_j(t), \mathbf{e}_{ij}, \mathbf{v}_i(t), \mathbf{v}_j(t)\right)$	$\mathbf{z}_i(t+1) = \phi_h\left(\mathbf{z}_i(t), \mathbf{m}_i(t)\right)$

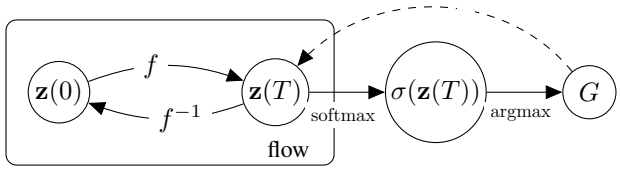

Figure 3: Plate diagram showing both the inference and generative components of `ModFlow`.

Earlier approaches use dequantisation to turn a graph G into a distribution of latent states, and argmax to deterministically map latent states to graphs (Zang and Wang, 2020).

We reduce the learning problem to maximizing the score cross-entropy $\mathbb{E}_{\hat{p}_{\text{data}}(\mathbf{z}(T))}[\log p_\theta(\mathbf{z}(T))]$, where we turn the observed set of graphs $\{G_n\}$ into a set of scores $\{\mathbf{z}_n\}$ by using one-hot encoding

$$\mathbf{z}_n(G_n; \epsilon) = (1-\epsilon)\ \text{onehot}(G_n)\ +\ \frac{\epsilon}{|\mathcal{A}_f|}\mathbf{1}_{M(n)}\mathbf{1}_{|\mathcal{A}_f|}^\top\ ,$$

where $\text{onehot}(G_n)$ is a matrix of size $M(n) \times |\mathcal{A}_f|$ (i.e., rows equal to number of nodes of G_n and columns equal to the number of possible node labels) such that $G_n(i,k) = 1$ if $v_i = a_k \in \mathcal{A}_f$, that is if the vertex i is labeled with atom k, and 0 otherwise; $\mathbf{1}_q$ is a vector with q entries each set to 1; $\mathcal{A}_f \in \{\mathcal{A}, \mathcal{A}_{\text{tree}}\}$; and $\epsilon \in [0,1]$ is added to model the noise in estimating the posterior $p(\mathbf{z}(T)|G)$ due to short-circuiting the inference process from G to $\mathbf{z}(T)$ skipping the intermediate dependencies, as shown in the plate diagram of Figure 3.

Effectively, we exploit the (non-reversible) composition of the argmax and softmax operations to transition from the continuous flow space to the discrete graph space, but skip this composition altogether in the reverse direction. Importantly, this short-circuiting allows `ModFlow` to keep the forward and backward flows between $\mathbf{z}(0)$ and $\mathbf{z}(T)$ completely aligned unlike previous approaches.

We thus maximize an objective over N training graphs,

$$\arg\max_\theta \quad \mathcal{L} = \mathbb{E}_{\hat{p}_{\text{data}}(\mathbf{z})} \log p_\theta(\mathbf{z}) \tag{8}$$

$$\approx \frac{1}{N}\sum_{n=1}^{N} \log p_T\big(\mathbf{z}(T) = \mathbf{z}_n\big) \tag{9}$$

$$= \frac{1}{N}\sum_{n=1}^{N}\left(\sum_{i=1}^{M(n)}\left[\log p_0(\mathbf{z}_i(0)) - \int_0^T \text{tr}\frac{\partial f_\theta(t, \mathbf{z}_i(t), \mathbf{z}_{\mathcal{N}_i}(t), \mathbf{x}_i, \mathbf{x}_{\mathcal{N}_i})}{\partial \mathbf{z}_i(t)} dt\right]\right), \tag{10}$$

which factorises over the size $M(n)$ of the n'th training molecule. The encoding probability follows from the flow Eq. 6, where $\mathbf{z}(0)$ is the reverse solution from $\mathbf{z}_n$ at time T following the flow f backward in time until $t = 0$. In practice we solve ODE integrals using numerical solvers, such as Runge-Kutta. We delegate this task to a general solver of the form $\texttt{ODESolve}(\mathbf{z}, f_\theta, T)$, where map f_θ is applied for T steps starting on $\mathbf{z}$. An optimizer `optim` is also required for updating θ.

Algorithm 1 Training `ModFlow`

Require: Dataset $\mathcal{D}$, iterations n_{iter}, batch size B, number of batches n_B

Initialise parameters θ of `ModFlow` (EGNN)
for $k = 1, \ldots, n_{\text{iter}}$ **do**
  for $b = 1, \ldots, n_B$ **do**
    Sample $\mathcal{D}_b = (G_1, \ldots, G_B) \sim \mathcal{D}$
    Init $\mathbf{z}_b(T)$ to $\mathbf{z}_b(G_b; \epsilon)$
    $\mathbf{z}_b(0) = \texttt{ODESolve}(\mathbf{z}_b(T), f_\theta, T)$
    $\mathcal{L}_b = \log p_\theta(G_b)$
  end for
  $\theta \leftarrow \texttt{optim}(\frac{1}{n_B} \sum_{b=1}^{n_B} \mathcal{L}_b; \theta)$
end for

Algorithm 2 Generating using `ModFlow`

$\mathbf{z}(0) \sim \mathcal{N}(0, I)$
$\mathbf{z}(T) = \texttt{ODESolve}(\mathbf{z}(0), f_\theta^{-1}, T)$
Assign labels by $\text{argmax}(\sigma(\mathbf{z}(T)))$

3.5 Molecular generation

We generate novel molecules by sampling an initial state $\mathbf{z}(0) \sim \mathcal{N}(0, I)$ based on structure, and running the modular flow forward in time until $\mathbf{z}(T)$. This procedure maps a tractable base distribution p_0 to some more complex distribution p_T. We follow argmax to pick the most probable label assignment for each node (Zang and Wang, 2020). The pseudo algorithms are shown in Algorithms 1 and 2.

4 Experiments

We evaluated `ModFlow` models trained, variously, on (i) 2D coordinates (ii) 3D coordinates (iii) 2D coordinates + Tree representation, (iv) 3D coordinates + Tree representation on the tasks of density estimation and molecular generation. We show that `ModFlow` compares favorably to other prominent flow and non-flow based molecular generative models including GraphDF (Luo et al., 2021), GraphNVP (Madhawa et al., 2019), MRNN(Popova et al., 2019), GraphAF (Shi et al., 2020) etc. Notably, `ModFlow` achieves state-of-the-art results without validity checks or post hoc correction. We also provide ablation results to underscore the relevance of geometric features and equivariance toward this superlative empirical performance.

4.1 Density Estimation

We now demonstrate the high expressive power of Modular Flows (`ModFlow`) on learning highly discontinuous patterns on 2D grid graphs.

We considered two variants of chessboard pattern as (i) 4×4 grid where every node has opposite value to its neighbors (ii) 16×16 grid where blocks of 4×4 nodes have uniform values, but opposite across blocks, and (iii) a 20×20 grid describing alternating stripes. Figure 4 shows that we can learn a neural differential f_θ function that reproduces the patterns almost perfectly, indicating sufficient capacity to model complex patterns. Our model is able to transform the initial Gaussian into multi-modal and discontinuous distributions.

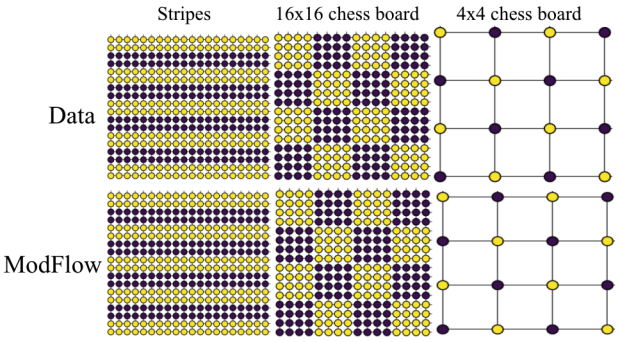

Figure 4: `ModFlow` can accurately learn to reproduce complex, discontinuous graph patterns.

4.2 Molecule Generation

Data. We train and evaluate the models on ZINC250k (Irwin et al., 2012) and QM9 (Ramakrishnan et al., 2014) datasets. The ZINC250k set contains 250,000 drug-like molecules up to 38 atoms. The QM9 set contains 134,000 stable small organic molecules consisting of `CHONF` atoms. The molecules are in kekulized form with hydrogens removed by the RDkit software (Landrum et al., 2013).

Setup. We adopt common quality metrics to evaluate molecular generation. (i) **Validity** is the fraction of molecules that satisfy chemical valency rule. In this work we strictly limit ourselves to comparing all methods on validity *without external correction procedures* (ii) **Uniqueness** is the fraction of non-duplicate generations, and (iii) **Novelty** is the fraction not present in training data. (iv) **Reconstruction** is the fraction of molecules that can be reconstructed from their encoding. We train the model over 5 different seed initialization, and generate 50,000 molecular graphs for evaluation. We report the mean and the standard deviation of the results from different seeds.

Implementation. The models are implemented in PyTorch (Paszke et al., 2019). The EGNN method used only a single layer with embedding dimension of 32. The input concatenates time and scalar vocabulary scores, per node. We train with Adam optimizer (Kingma and Ba, 2014), for 50-100 epochs with batch size 1000 and learning rate 0.001. For more details, see Appendix A.4.

Results. Tables 3 and 4 show the results on QM9 and ZINC250K. `ModFlow` achieves state-of-the-art results across all metrics. Notably, its reconstruction rate is 100% similar to other flow models; in addition, however, novelty (100%) and uniqueness scores (99%) are also very high. Moreover, `ModFlow` surpassed all early methods on validity (95%-99%). These results underscore the promise of `ModFlow`as an effective tool for graph density estimation and molecular generation. Additional evaluation metrics, property optimization and comparison with properties distribution are shown in Appendix A.6 and A.7

Table 3: Random generation performance on QM9 dataset without post-hoc validity corrections. Results with * are taken from Luo et al. (2021). Higher values are better for all columns.

Method	Validity %	Uniqueness %	Novelty %	Reconstruction %
GVAE	60.2	9.3	80.9	96.0
GraphNVP*	83.1	99.2	58.2	100
GRF*	84.5	66	58.6	100
GraphAF*	67	94.2	88.8	100
GraphDF*	82.7	97.6	98.1	100
MoFlow*	89.0	98.5	96.4	100
`ModFlow` (2D-EGNN)	**96.2** $\pm$ 1.7	**99.5**	**100**	100
`ModFlow` (3D-EGNN)	**98.3** $\pm$ 0.7	99.1	**100**	100
`ModFlow` (JT-2D-EGNN)	**97.9** $\pm$ 1.2	99.2	**100**	100
`ModFlow` (JT-3D-EGNN)	**99.1** $\pm$ 0.8	99.3	**100**	100

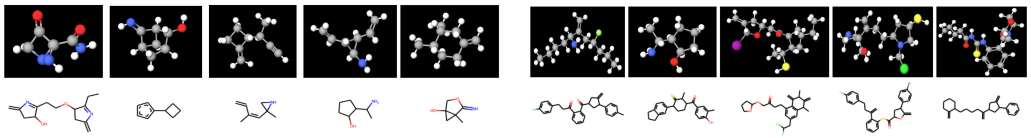

(a) QM9 Dataset (b) ZINC250K Dataset

Figure 5: Samples of molecules generated by `ModFlow`. More examples are shown in Appendix A.8.

4.3 Ablation Studies

We performed ablation experiments to gain further insights about `ModFlow`, as described next.

Table 4: Random generation performance on ZINC250K dataset without post-hoc validity corrections. Results with * are taken from Luo et al. (2021). Higher values are better for all columns.

Method	Validity %	Uniqueness %	Novelty %	Reconstruction %
MRNN	65	99.89	100	n/a
GVAE	7.2	9	100	53.7
GCPN	20	99.97	100	n/a
GraphNVP*	42.6	94.8	100	100
GRF*	73.4	53.7	100	100
GraphAF*	68	99.1	100	100
GraphDF*	89	99.2	100	100
MoFlow*	50.3	**99.9**	100	100
`ModFlow` (2D-EGNN)	**94.8** ± 1.0	99.4	100	100
`ModFlow` (3D-EGNN)	**95.4** ± 1.2	99.7	100	100
`ModFlow` (JT-2D-EGNN)	**97.4** ± 1.4	99.1	100	100
`ModFlow` (JT-3D-EGNN)	**98.1** ± 0.9	99.3	100	100

E(3) Equivariant vs Not Equivariant. Molecules exhibit translational and rotational symmetries, so we conducted an ablation study to quantify the effect of incorporating these symmetries in our model. We compare the results obtained via using EGNN to non-equivariant graph convolutional networks (GCN). We used a 3-layer GCN with layer sizes 64-32-32. Table 5 provides strong evidence in favor of modeling symmetries explicitly in Modular Flows.

Table 5: Random generation performance on ZINC250K and QM9 dataset with E(3)-EGNN vs GCN.

Dataset	Method	Validity %	Uniqueness %	Novelty %
ZINC250K	`ModFlow` (3D-EGNN)	95.4 ± 1.2	99.7	100
	`ModFlow` (GCN)	90.3 ± 1.9	99.7	100
QM9	`ModFlow` (3D-EGNN)	98.3 ± 0.7	99.1	100
	`ModFlow` (GCN)	93.3 ± 0.5	98.8	100

2D vs 3D. Finally, we study whether including 3D coordinate information improves the model. The EGNN coupled differential function obtains either the 2D or 3D positions as polar coordinates, whereas 3D has an extra degree of freedom. Table 6 shows that transitioning to 3D gives a consistent $\approx 2\%$ percentage unit performance improvement with respect to validity.

Table 6: Random generation performance on ZINC250K and QM9 dataset with 2D vs 3D features

Dataset	Method	Validity %	Uniqueness %	Novelty %
ZINC250K	`ModFlow` (3D-EGNN)	95.4 ± 1.2	99.7	100
	`ModFlow` (2D-EGNN)	94.8 ± 1.0	99.4	100
QM9	`ModFlow` (3D-EGNN)	98.3 ± 0.7	99.1	100
	`ModFlow` (2D-EGNN)	96.2 ± 1.7	99.5	100

5 Conclusion

We proposed `ModFlow`, a new generative flow model where multiple flows interact locally according to a coupled ODE, resulting in accurate modeling of graph densities and high quality molecular generation without any validity checks or correction.

Interesting avenues open up, including the design of (a) more nuanced mappings between discrete and continuous spaces, and (b) extensions of modular flows to (semi-)supervised settings.

References

James Atwood and Don Towsley. Diffusion-convolutional neural networks. *Advances in neural information processing systems*, 29, 2016.

G Richard Bickerton, Gaia V Paolini, Jérémy Besnard, Sorel Muresan, and Andrew L Hopkins. Quantifying the chemical beauty of drugs. *Nature chemistry*, 4(2):90–98, 2012.

Andrew M. Bradley. PDE-constrained optimization and the adjoint method. Technical report, 2019.

Ben Chamberlain, James Rowbottom, Maria I Gorinova, Michael Bronstein, Stefan Webb, and Emanuele Rossi. Grand: Graph neural diffusion. In *International Conference on Machine Learning*, pages 1407–1418. PMLR, 2021.

Ricky TQ Chen, Yulia Rubanova, Jesse Bettencourt, and David K Duvenaud. Neural ordinary differential equations. *Advances in neural information processing systems*, 31, 2018.

Eike Cramer, Alexander Mitsos, Raul Tempone, and Manuel Dahmen. Principal component density estimation for scenario generation using normalizing flows, 2021. URL `https://arxiv.org/abs/2104.10410`.

Hanjun Dai, Yingtao Tian, Bo Dai, Steven Skiena, and Le Song. Syntax-directed variational autoencoder for structured data, 2018. URL `https://arxiv.org/abs/1802.08786`.

Laurent Dinh, David Krueger, and Yoshua Bengio. Nice: Non-linear independent components estimation. *arXiv preprint arXiv:1410.8516*, 2014.

Laurent Dinh, Jascha Sohl-Dickstein, and Samy Bengio. Density estimation using real nvp. *arXiv preprint arXiv:1605.08803*, 2016.

Moshe Eliasof, Eldad Haber, and Eran Treister. Pde-gcn: Novel architectures for graph neural networks motivated by partial differential equations. *Advances in Neural Information Processing Systems*, 34, 2021.

Peter Ertl and Ansgar Schuffenhauer. Estimation of synthetic accessibility score of drug-like molecules based on molecular complexity and fragment contributions. *Journal of cheminformatics*, 1(1):1–11, 2009.

Vikas Garg, Stefanie Jegelka, and Tommi Jaakkola. Generalization and representational limits of graph neural networks. In *Proceedings of the 37th International Conference on Machine Learning, ICML 2020, 13-18 July 2020, Virtual Event*, volume 119 of *Proceedings of Machine Learning Research*, pages 3419–3430. PMLR, 2020. URL `http://proceedings.mlr.press/v119/garg20c.html`.

Ian J. Goodfellow, Jean Pouget-Abadie, Mehdi Mirza, Bing Xu, David Warde-Farley, Sherjil Ozair, Aaron Courville, and Yoshua Bengio. Generative adversarial networks, 2014. URL `https://arxiv.org/abs/1406.2661`.

Will Grathwohl, Ricky TQ Chen, Jesse Bettencourt, Ilya Sutskever, and David Duvenaud. Ffjord: Free-form continuous dynamics for scalable reversible generative models. *arXiv preprint arXiv:1810.01367*, 2018.

Shion Honda, Hirotaka Akita, Katsuhiko Ishiguro, Toshiki Nakanishi, and Kenta Oono. Graph residual flow for molecular graph generation. *arXiv preprint arXiv:1909.13521*, 2019.

Chin-Wei Huang, David Krueger, Alexandre Lacoste, and Aaron Courville. Neural autoregressive flows, 2018. URL `https://arxiv.org/abs/1804.00779`.

Valerii Iakovlev, Markus Heinonen, and Harri Lähdesmäki. Learning continuous-time pdes from sparse data with graph neural networks. *arXiv preprint arXiv:2006.08956*, 2020.

John Ingraham, Vikas Garg, Regina Barzilay, and Tommi Jaakkola. Generative models for graph-based protein design. In H. Wallach, H. Larochelle, A. Beygelzimer, F. d'Alché-Buc, E. Fox, and R. Garnett, editors, *Advances in Neural Information Processing Systems*, volume 32. Curran Associates, Inc., 2019. URL `https://proceedings.neurips.cc/paper/2019/file/f3a4ff4839c56a5f460c88cce3666a2b-Paper.pdf`.

John J Irwin, Teague Sterling, Michael M Mysinger, Erin S Bolstad, and Ryan G Coleman. Zinc: a free tool to discover chemistry for biology. *Journal of chemical information and modeling*, 52(7):1757–1768, 2012.

Wengong Jin, Regina Barzilay, and Tommi Jaakkola. Junction tree variational autoencoder for molecular graph generation. *arXiv preprint arXiv:1802.04364*, 2018.

Hiroshi Kajino. Molecular hypergraph grammar with its application to molecular optimization. In *International Conference on Machine Learning*, pages 3183–3191. PMLR, 2019.

Diederik P Kingma and Jimmy Ba. Adam: A method for stochastic optimization. *arXiv preprint arXiv:1412.6980*, 2014.

Diederik P Kingma and Max Welling. Auto-encoding variational bayes, 2013. URL https://arxiv.org/abs/1312.6114.

Ivan Kobyzev, Simon J.D. Prince, and Marcus A. Brubaker. Normalizing flows: An introduction and review of current methods. *IEEE Transactions on Pattern Analysis and Machine Intelligence*, 43(11):3964–3979, nov 2021. doi: 10.1109/tpami.2020.2992934. URL https://doi.org/10.1109%2Ftpami.2020.2992934.

Andrei Nikolaevich Kolmogorov, Ye F Mishchenko, and Lev Semenovich Pontryagin. A probability problem of optimal control. Technical report, JOINT PUBLICATIONS RESEARCH SERVICE ARLINGTON VA, 1962.

Matt J. Kusner, Brooks Paige, and José Miguel Hernández-Lobato. Grammar variational autoencoder, 2017. URL https://arxiv.org/abs/1703.01925.

Greg Landrum et al. Rdkit: A software suite for cheminformatics, computational chemistry, and predictive modeling, 2013.

Zongyi Li, Nikola Kovachki, Kamyar Azizzadenesheli, Burigede Liu, Kaushik Bhattacharya, Andrew Stuart, and Anima Anandkumar. Neural operator: Graph kernel network for partial differential equations. *arXiv preprint arXiv:2003.03485*, 2020.

Jaechang Lim, Seongok Ryu, Jin Woo Kim, and Woo Youn Kim. Molecular generative model based on conditional variational autoencoder for de novo molecular design. *Journal of cheminformatics*, 10(1):1–9, 2018.

Phillip Lippe and Efstratios Gavves. Categorical normalizing flows via continuous transformations. In *International Conference on Learning Representations*, 2021. URL https://openreview.net/forum?id=-GLNZeVDuik.

Youzhi Luo, Keqiang Yan, and Shuiwang Ji. Graphdf: A discrete flow model for molecular graph generation, 2021. URL https://arxiv.org/abs/2102.01189.

Kaushalya Madhawa, Katushiko Ishiguro, Kosuke Nakago, and Motoki Abe. Graphnvp: An invertible flow model for generating molecular graphs. *arXiv preprint arXiv:1905.11600*, 2019.

Lukasz Maziarka, Agnieszka Pocha, Jan Kaczmarczyk, Krzysztof Rataj, Tomasz Danel, and Michał Warchoł. Mol-cyclegan: a generative model for molecular optimization. *Journal of Cheminformatics*, 12(1):1–18, 2020.

Kenneth M. Merz, Gianni De Fabritiis, and Guo-Wei Wei. Generative models for molecular design. *Journal of Chemical Information and Modeling*, 60(12):5635–5636, 2020. doi: 10.1021/acs.jcim.0c01388. URL https://doi.org/10.1021/acs.jcim.0c01388. PMID: 33378853.

Daniel Neil, Marwin Segler, Laura Guasch, Mohamed Ahmed, Dean Plumbley, Matthew Sellwood, and Nathan Brown. Exploring deep recurrent models with reinforcement learning for molecule design. 2018.

George Papamakarios, Eric Nalisnick, Danilo Jimenez Rezende, Shakir Mohamed, and Balaji Lakshminarayanan. Normalizing flows for probabilistic modeling and inference. *Journal of Machine Learning Research*, 22(57): 1–64, 2021.

Adam Paszke, Sam Gross, Francisco Massa, Adam Lerer, James Bradbury, Gregory Chanan, Trevor Killeen, Zeming Lin, Natalia Gimelshein, Luca Antiga, et al. Pytorch: An imperative style, high-performance deep learning library. *Advances in neural information processing systems*, 32, 2019.

Michael Poli, Stefano Massaroli, Junyoung Park, Atsushi Yamashita, Hajime Asama, and Jinkyoo Park. Graph neural ordinary differential equations. *arXiv preprint arXiv:1911.07532*, 2019.

Pavel G Polishchuk, Timur I Madzhidov, and Alexandre Varnek. Estimation of the size of drug-like chemical space based on gdb-17 data. *Journal of computer-aided molecular design*, 27(8):675–679, 2013.

Daniil Polykovskiy, Alexander Zhebrak, Benjamin Sanchez-Lengeling, Sergey Golovanov, Oktai Tatanov, Stanislav Belyaev, Rauf Kurbanov, Aleksey Artamonov, Vladimir Aladinskiy, Mark Veselov, Artur Kadurin, Simon Johansson, Hongming Chen, Sergey Nikolenko, Alan Aspuru-Guzik, and Alex Zhavoronkov. Molecular Sets (MOSES): A Benchmarking Platform for Molecular Generation Models. *Frontiers in Pharmacology*, 2020.

Mariya Popova, Mykhailo Shvets, Junier Oliva, and Olexandr Isayev. Molecularrnn: Generating realistic molecular graphs with optimized properties, 2019. URL https://arxiv.org/abs/1905.13372.

Kristina Preuer, Philipp Renz, Thomas Unterthiner, Sepp Hochreiter, and Gunter Klambauer. Fréchet chemnet distance: a metric for generative models for molecules in drug discovery. *Journal of chemical information and modeling*, 58(9):1736–1741, 2018.

Raghunathan Ramakrishnan, Pavlo O Dral, Matthias Rupp, and O Anatole von Lilienfeld. Quantum chemistry structures and properties of 134 kilo molecules. *Scientific Data*, 1, 2014.

Aditya Ramesh, Prafulla Dhariwal, Alex Nichol, Casey Chu, and Mark Chen. Hierarchical text-conditional image generation with clip latents, 2022. URL https://arxiv.org/abs/2204.06125.

Emanuele Rossi, Ben Chamberlain, Fabrizio Frasca, Davide Eynard, Federico Monti, and Michael Bronstein. Temporal graph networks for deep learning on dynamic graphs, 2020. URL https://arxiv.org/abs/2006.10637.

Bidisha Samanta, Abir De, Niloy Ganguly, and Manuel Gomez-Rodriguez. Designing random graph models using variational autoencoders with applications to chemical design. *arXiv preprint arXiv:1802.05283*, 2018.

Victor Garcia Satorras, Emiel Hoogeboom, and Max Welling. E(n) equivariant graph neural networks, 2021. URL https://arxiv.org/abs/2102.09844.

Franco Scarselli, Marco Gori, Ah Chung Tsoi, Markus Hagenbuchner, and Gabriele Monfardini. The graph neural network model. *IEEE Transactions on Neural Networks*, 20(1):61–80, 2009. doi: 10.1109/TNN.2008.2005605.

Marwin HS Segler, Thierry Kogej, Christian Tyrchan, and Mark P Waller. Generating focused molecule libraries for drug discovery with recurrent neural networks. *ACS central science*, 4(1):120–131, 2018.

Chence Shi, Minkai Xu, Zhaocheng Zhu, Weinan Zhang, Ming Zhang, and Jian Tang. Graphaf: a flow-based autoregressive model for molecular graph generation. *arXiv preprint arXiv:2001.09382*, 2020.

Jonathan M. Stokes, Kevin Yang, Kyle Swanson, Wengong Jin, Andres Cubillos-Ruiz, Nina M. Donghia, Craig R. MacNair, Shawn French, Lindsey A. Carfrae, Zohar Bloom-Ackermann, Victoria M. Tran, Anush Chiappino-Pepe, Ahmed H. Badran, Ian W. Andrews, Emma J. Chory, George M. Church, Eric D. Brown, Tommi S. Jaakkola, Regina Barzilay, and James J. Collins. A deep learning approach to antibiotic discovery. *Cell*, 180(4):688–702.e13, 2020. ISSN 0092-8674. doi: https://doi.org/10.1016/j.cell.2020.01.021. URL https://www.sciencedirect.com/science/article/pii/S0092867420301021.

David Weininger. Smiles, a chemical language and information system. 1. introduction to methodology and encoding rules. *Journal of chemical information and computer sciences*, 28(1):31–36, 1988.

Scott A Wildman and Gordon M Crippen. Prediction of physicochemical parameters by atomic contributions. *Journal of chemical information and computer sciences*, 39(5):868–873, 1999.

Louis-Pascal Xhonneux, Meng Qu, and Jian Tang. Continuous graph neural networks. In *International Conference on Machine Learning*, pages 10432–10441. PMLR, 2020.

Jiaxuan You, Rex Ying, Xiang Ren, William Hamilton, and Jure Leskovec. Graphrnn: Generating realistic graphs with deep auto-regressive models. In *International conference on machine learning*, pages 5708–5717. PMLR, 2018.

Chengxi Zang and Fei Wang. Moflow: an invertible flow model for generating molecular graphs. In *Proceedings of the 26th ACM SIGKDD International Conference on Knowledge Discovery & Data Mining*, pages 617–626, 2020.

Xingjian Zhen, Rudrasis Chakraborty, Liu Yang, and Vikas Singh. Flow-based generative models for learning manifold to manifold mappings, 2020. URL https://arxiv.org/abs/2012.10013.

A Appendix

A.1 Tree Decomposition

The tree decomposition of the molecules follow closely to Jin et al. (2018) described algorithm. The rings in the molecule are extracted by RDKit's `GetRingInfo, GetSymmSSSR` function, where it provides the nodes corresponding to the ring sub-structure including the merged rings also. We constrain our clusters (vocabulary) to be unique ring-substructures present in the molecules. It is observed vocabulary of clusters, follows a skewed distribution over frequency of appearance within dataset. It means that only a subset (~ 30) of ring-substructures (labels) have high frequency of appearance within any molecule as compared to other substructures within the vocabulary. We simplify the vocabulary by only representing the 30 commonly occurring substructures of $\mathcal{A}_{tree}$. In Figure 6 , we have shown examples of cluster vocabulary of ring-substructure for different datasets.

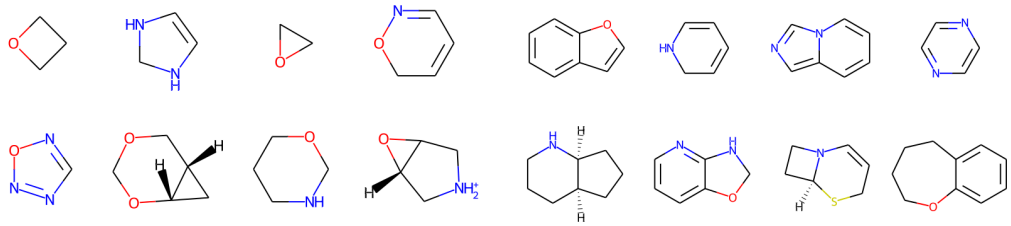

(a) QM9 Dataset (b) ZINC250K Dataset

Figure 6: Examples of cluster vocabulary

A.2 Equivariant Graph Neural Networks (EGNN)

Equivariant Graph Neural Networks (Satorras et al., 2021) are a class of GNN which are translation, rotation and reflection equivariant (E(n)), and permutation equivariant with respect to an input set of points. These symmetries corresponds to E(3) group which can be extended to E(n) group. For input the set of node embeddings $\mathbf{h}^l = \{\mathbf{h}_0^l, \mathbf{h}_1^l, ..., \mathbf{h}_{M-1}^l\}$ and coordinate embeddings $\mathbf{x}^l = \{\mathbf{x}_0^l, \mathbf{x}_1^l, ..., \mathbf{x}_{M-1}^l\}$ and edge information E = (a_{ij}) and outputs a transformation on $\mathbf{h}^{l+1}$ and $\mathbf{x}^{l+1}$ as:

$$\mathbf{m}_{ij} = \phi_e\left(\mathbf{h}_i^l, \mathbf{h}_j^l, \left\|\mathbf{x}_i^l - \mathbf{x}_j^l\right\|^2, a_{ij}\right) \tag{11}$$

$$\mathbf{x}_i^{l+1} = \mathbf{x}_i^l + C\sum_{j\neq i}\left(\mathbf{x}_i^l - \mathbf{x}_j^l\right)\phi_x\left(\mathbf{m}_{ij}\right) \tag{12}$$

$$\mathbf{m}_i = \sum_{j\neq i}\mathbf{m}_{ij} \tag{13}$$

$$\mathbf{h}_i^{l+1} = \phi_h\left(\mathbf{h}_i^l, \mathbf{m}_i\right) \tag{14}$$

Here, the edge operation ϕ_e also take input the relative squared distance between two coordinates $\left\|\mathbf{x}_i^l - \mathbf{x}_j^l\right\|^2$, with node embeddings $\mathbf{h}_i^l, \mathbf{h}_j^l$ and edge attribute a_{ij}. Subsequently, position of each node $\mathbf{x}_i^l$ is updated via a vector field in a radial direction. This means that, the position is updated by the weighted sum of all relative differences $(\mathbf{x}_i - \mathbf{x}_j)_{\forall j}$ by function ϕ_x. C is chosen to be $1/(M-1)$, which divides the sum by its number of elements. The Eq. 18 is the aggregation step, which can be limited to the neighbourhood $j \in \mathcal{N}(i)$ and Eq. 19 performs node operation ϕ_h. In case, when dealing with static coordinates $\mathbf{x}_i$ this becomes E(n) invariant.

A.3 Connection to Temporal Graph Networks

Temporal Graph Networks (Rossi et al., 2020) belong to class of methods applied on dynamic graphs. Specifically, it consist of combination of memory modules and graph-based operators acting as a neural model for dynamic graphs. First, for an event a message $\mathbf{m}_i'(t)$ is computed to update i's memory using previous time-step memory state ($\mathbf{s}_i\left(t^-\right)$). The msg is a learnable function like MLP, which aggregates the messages $\mathbf{m}_i'(t_1), \mathbf{m}_i'(t_2), ..., \mathbf{m}_i'(t_b)$ for $t_1, t_2.....t_b \leq t$. The aggregated message $\overline{\mathbf{m}}_i'(t)$ is then used to update the memory state of the node. Various choices of network architecture like RNNs, MLP etc can be incorporated as agg or mem. Finally, the node embeddings are updated as a summation over the neighbouring nodes $n_i^k([0,t])$, where h is a learnable function. The operations are listed in Table 7 respectively.

EGNN inherently does not have any time-dynamics, but when combined with modular flows it can be treated as a temporal EGNN, which can be casted as a variant of TGN. In Table 7, we have summarized the dynamics of both the architectures, and devised a mapping from one to another. From the above, we can see similarity in term of operations between two networks.

Table 7: Comparison and mapping of TGN to our method. We use the shorthand $\mathbf{r}_{ij} = (\mathbf{x}_i - \mathbf{x}_j)$, a_{ij} are the edge attributes, $\mathbf{s}_i$ is memory state of node (TGN) and $\mathbf{v}_i, \mathbf{e}_{ij}$ are node and edge features.

Method	TGN layer	`ModFlow`
Edge	$\mathbf{m}_i'(t) = \mathrm{msg}\left(\mathbf{s}_i\left(t^-\right), t, \mathbf{v}_i(t)\right)$ $\overline{\mathbf{m}}_i'(t) = \mathrm{agg}\left(\mathbf{m}_i'\left(t_1\right), \ldots, \mathbf{m}_i'\left(t_b\right)\right)$	$\mathbf{m}_{ij}(t) = \phi_e\left(\mathbf{z}_i(t), \mathbf{z}_j(t), \left\|\mathbf{r}_{ij}(t)\right\|^2, a_{ij}\right)$ $\hat{\mathbf{m}}_{ij}(t) = \mathbf{r}_{ij}(t) \cdot \phi_x\left(\mathbf{m}_{ij}(t)\right)$ $\mathbf{m}_i(t) = \sum_{j \in \mathcal{N}(i)} \mathbf{m}_{ij}$ $\hat{\mathbf{m}}_i(t) = C \cdot \sum_{j \in \mathcal{N}(i)} \hat{\mathbf{m}}_{ij}(t)$
Memory state	$\mathbf{s}_i(t) = \mathrm{mem}\left(\overline{\mathbf{m}}_i'(t), \mathbf{s}_i\left(t^-\right)\right)$	$\mathbf{x}_i(t+1) = \mathbf{x}_i(t) + \hat{\mathbf{m}}_i(t)$
Node	$\mathbf{z}_i'(t) = \sum_{j \in n_i^k([0,t])} h\left(\mathbf{s}_i(t), \mathbf{s}_j(t), \mathbf{e}_{ij}, \mathbf{v}_i(t), \mathbf{v}_j(t)\right)$	$\mathbf{z}_i(t+1) = \phi_h\left(\mathbf{z}_i(t), \mathbf{m}_i(t)\right)$

The role of the memory state $\mathbf{s}_i$ in TGN can be played by coordinate embeddings $\mathbf{x}_i$ in our method and messages can be formulated with respect to both in the networks. It is worthy to note that TGN also incorporates neighbouring node attributes, memory states to update the node embedding $\mathbf{z}_i'$ which is the similar to ours where the aggregated message over neighbouring nodes is used to update the node embedding $\mathbf{z}_i$, where (ϕ_h) is a learnable function. From the above similarities, we can see that the our method can be casted as a variant of TGN, which is also equivariant as compared to TGN.

A.4 Implementation Details

The model is implemented in PyTorch (Paszke et al., 2019). The EGNN implementation consist of 1 layer, and the embedding dimension is 32 and the neighbourhood is restricted to 1-hop neighbours of each node. The input are the node embeddings and the coordinate positions in polar coordinates (2D) and spherical polar coordinates (3D). The input dimension is the size of the vocabulary being considered with time concatenated to the input embedding. We solve the ODE system with Dormand–Prince adaptive step size scheme `dopri5` adaptive ODE solver, and the number of function evaluations lie roughly between $70 \sim 100$. Adam (Kingma and Ba, 2014) optimizer is used to train the model. Model is trained for 50 - 100 epochs. The training time of our model slightly above some one-shot discrete flows model where a single flow is characterizing whole system as compared to ours where each node has its own ODE. However, the training time is less than as compared to the Auto-regressive methods

Computational time is a crucial aspect for generative modeling involved in huge search spaces like molecules. We have compared the computational time (excluding preprocessing time) for generation of a molecule for ZINC250k and QM9 dataset reported in Table 8. The time is initially computed via generating 10000 molecules, then averaged across 5 runs. Notably, `ModFlow` is a one-hot generation model which is faster in order of magnitude from the auto-regressive models like GraphAF and GraphDF. However, the computational time depends heavily on the choices of frameworks and skills of implementations. `ModFlow` poses faster sampling time similar to any one-shot sampling technique and does not involve any additional validity checks and does not require multiple decoding like in JT-VAE.

Table 8: Generation time of various models performed on QM9 and ZINC250K dataset. Time is in seconds denoted as $\mathcal{O}$(second/molecule)

Method	ZINC250K	QM9
GraphEBM	1.12 ± 0.34	0.53 ± 0.16
GVAE	0.86 ± 0.12	0.46 ± 0.07
GraphAF	0.93 ± 0.14	0.56 ± 0.12
GraphDF	3.12 ± 0.56	1.92 ± 0.42
MoFlow	0.71 ± 0.14	0.31 ± 0.04
`ModFlow` (2D-EGNN)	0.46 ± 0.09	0.16 ± 0.04
`ModFlow` (3D-EGNN)	0.55 ± 0.13	0.24 ± 0.06
`ModFlow` (JT-2D-EGNN)	0.53 ± 0.07	0.21 ± 0.07
`ModFlow` (JT-3D-EGNN)	0.62 ± 0.11	0.28 ± 0.09

A.5 Derivation of modular adjoint

We present a standard adjoint gradient derivation (Bradley, 2019), and show that the adjoint of a graph neighborhood differential is sparse.

For completeness, we define an ODE system

$$\dot{\mathbf{z}}(t) = f(\mathbf{z}, t, \boldsymbol{\theta}) \tag{15}$$

$$\mathbf{z}(t) = \mathbf{z}_0 + \int_0^t f(\mathbf{z}, t, \boldsymbol{\theta}) d\tau, \tag{16}$$

where $\mathbf{z} \in \mathbb{R}^D$ is a state vector, $\dot{\mathbf{z}} \in \mathbb{R}^D$ is the state time differential defined by the vector field function f and parameterised by $\boldsymbol{\theta}$. The starting state is $\mathbf{z}_0$, and $t, \tau \in \mathbb{R}_+$ are time variables. Our goal is to solve a constrained problem

$$\min_{\boldsymbol{\theta}} \quad G(\boldsymbol{\theta}) = \int_0^T g(\mathbf{z}, t, \boldsymbol{\theta}) dt \tag{17}$$

$$s.t. \quad \dot{\mathbf{z}} - f(\mathbf{z}, t, \boldsymbol{\theta}) = 0, \qquad \forall t \in [0, T] \tag{18}$$

$$\mathbf{z}(0) - \mathbf{z}_0 = 0, \tag{19}$$

where G is the total loss that consists of instant loss functionals g. We desire to compute the gradients of the system $\nabla_{\boldsymbol{\theta}} G$.

We optimise the constrained problem by solving the Lagrangian

$$\mathcal{L}(\boldsymbol{\theta}, \boldsymbol{\lambda}, \boldsymbol{\mu}) = G(\boldsymbol{\theta}) + \int_0^T \boldsymbol{\lambda}(t)^\top (\dot{\mathbf{z}} - f(\mathbf{z}, t, \boldsymbol{\theta})) dt + \boldsymbol{\mu}^\top (\mathbf{z}(0) - \mathbf{z}_0) \tag{20}$$

$$= \int_0^T \Big[g(\mathbf{z}, t, \boldsymbol{\theta}) + \boldsymbol{\lambda}(t)^\top (\dot{\mathbf{z}} - f(\mathbf{z}, t, \boldsymbol{\theta})) \Big] dt + \boldsymbol{\mu}^\top (\mathbf{z}(0) - \mathbf{z}_0) \ . \tag{21}$$

The constraints are satisfied by the ODE definition. Hence, $\nabla_{\boldsymbol{\theta}} \mathcal{L} = \nabla_{\boldsymbol{\theta}} G$, and we can set values $\boldsymbol{\theta}$ and $\boldsymbol{\mu}$ freely. We use a shorthand notation $\frac{\partial a}{\partial b} = a_b$, and omit parameters from the functions for notational simplicity. Applying the chain rule, we note that the gradient becomes

$$\nabla_{\boldsymbol{\theta}} \mathcal{L} = \nabla_{\boldsymbol{\theta}} G = \int_0^T \Big[g_{\mathbf{z}} \mathbf{z}_{\boldsymbol{\theta}} + g_{\boldsymbol{\theta}} + \boldsymbol{\lambda}^\top \dot{\mathbf{z}}_{\boldsymbol{\theta}} - \boldsymbol{\lambda}^\top f_{\mathbf{z}} \mathbf{z}_{\boldsymbol{\theta}} - \boldsymbol{\lambda}^\top f_{\boldsymbol{\theta}} \Big] dt \ , \tag{22}$$

where the $\boldsymbol{\mu}$ term drops out since it does not depend on parameters $\boldsymbol{\theta}$. We apply integration by parts to swap the differentials in term $\boldsymbol{\lambda}^\top \dot{\mathbf{z}}_{\boldsymbol{\theta}}$, resulting in

$$\int_0^T \boldsymbol{\lambda}^\top \dot{\mathbf{z}}_{\boldsymbol{\theta}} dt = \boldsymbol{\lambda}^\top \mathbf{z}_{\boldsymbol{\theta}}|_{t=T} - \boldsymbol{\lambda}^\top \mathbf{z}_{\boldsymbol{\theta}}|_{t=0} - \int_0^T \dot{\boldsymbol{\lambda}}^\top \mathbf{z}_{\boldsymbol{\theta}} dt \ . \tag{23}$$

Substituting this into previous equation and rearranging the terms results in

$$\nabla_{\boldsymbol{\theta}} \mathcal{L} = \int_0^T \underbrace{(g_{\mathbf{z}} - \boldsymbol{\lambda}^\top f_{\mathbf{z}} - \dot{\boldsymbol{\lambda}}^\top) \mathbf{z}_{\boldsymbol{\theta}}}_{0, \text{ if } \dot{\boldsymbol{\lambda}}^\top = g_{\mathbf{z}} - \boldsymbol{\lambda}^\top f_{\mathbf{z}}} dt + \int_0^T (g_{\boldsymbol{\theta}} - \boldsymbol{\lambda}^\top f_{\boldsymbol{\theta}}) dt + \underbrace{\boldsymbol{\lambda}^\top \mathbf{z}_{\boldsymbol{\theta}}|_{t=T}}_{0, \text{ if } \boldsymbol{\lambda}(T) = \mathbf{0}} - \underbrace{\boldsymbol{\lambda}^\top \mathbf{z}_{\boldsymbol{\theta}}|_{t=0}}_{0} . \tag{24}$$

The last term is removed since $\mathbf{z}(0)$ not depend on $\boldsymbol{\theta}$ as a constant, and thus $\mathbf{z}_{\boldsymbol{\theta}}(0) = 0$. The difficult term in the equation is $\mathbf{z}_{\boldsymbol{\theta}}$. We remove it by choosing

$$\dot{\boldsymbol{\lambda}}^{\top} = g_{\mathbf{z}} - \boldsymbol{\lambda}^{\top} f_{\mathbf{z}}. \tag{25}$$

Finally, we choose $\boldsymbol{\lambda}(T) = 0$ which also removes the second-to-last term. The choices lead to a final term

$$\nabla_{\boldsymbol{\theta}} G = \nabla_{\boldsymbol{\theta}} \mathcal{L} = \int_0^T (g_{\boldsymbol{\theta}} - \boldsymbol{\lambda}^{\top} f_{\boldsymbol{\theta}}) dt \tag{26}$$

$$s.t. \quad \dot{\boldsymbol{\lambda}}^{\top} = g_{\mathbf{z}} - \boldsymbol{\lambda}^{\top} f_{\mathbf{z}} \tag{27}$$

$$\boldsymbol{\lambda}(T) = 0. \tag{28}$$

In the derivation the adjoint $\boldsymbol{\lambda}(t) = \frac{\partial \mathcal{L}}{\partial \mathbf{z}(t)} \in \mathbb{R}^D$ represents the change of loss with respect to instant states, and is another ODE system that runs backwards from $\boldsymbol{\lambda}(T) = 0$ until $\boldsymbol{\lambda}(0)$. The final gradient $\nabla_{\boldsymbol{\theta}} \mathcal{L}$ counts all adjoints within $[0, T]$ multiplied by the 'immediate' partial derivatives $f_{\boldsymbol{\theta}}$. The final gradient also takes into account the instant loss parameter derivatives. For simple MSE curve fitting, the instant loss has no parameters. The adjoint depends on the instant loss state derivatives $g_{\mathbf{z}}$. These are often only available for observations $\mathbf{y}_j$ at observed timepoints t_j. This can be represented by having a convenient loss

$$g(\mathbf{z}, t, \boldsymbol{\theta}) = \delta(t = t_j) \tilde{g}(\mathbf{z}, \mathbf{y}_j, t, \boldsymbol{\theta}), \tag{29}$$

and now the term $g_{\mathbf{z}}$ induces discontinuous jumps at observations. This does not pose problems in practice, since we can integrate the ODE in continuous segments between the observation instants.

The sparsity of the adjoint evolution is evident from the equation 27, where the $\dot{\boldsymbol{\lambda}}_i$ is an inner product between $\boldsymbol{\lambda}$ and one column of $\frac{\partial f}{\partial \mathbf{z}}$, which is invariant to non-neighbors. This gives a result

$$\frac{d\boldsymbol{\lambda}_i}{dt} = -\boldsymbol{\lambda}(t)^{\top} \frac{\partial f\big(t, \mathbf{z}_i(t), \mathbf{z}_{\mathcal{N}_i}(t), \mathbf{x}_i, \mathbf{x}_{\mathcal{N}_i}\big)}{\partial \mathbf{z}} = -\sum_{j \in \mathcal{N}_i \cup \{i\}} \boldsymbol{\lambda}_j(t)^{\top} \frac{\partial f\big(t, \mathbf{z}_i(t), \mathbf{z}_{\mathcal{N}_i}(t), \mathbf{x}_i, \mathbf{x}_{\mathcal{N}_i}\big)}{\partial \mathbf{z}_j}. \tag{30}$$

A.6 Additional Evaluation Metrics

We have performed additional metric evaluations to evaluate `ModFlow` capability to generate molecules. We evaluate our model against the MOSES(Polykovskiy et al., 2020) metrics and compared it with existing methods. These metrics access the overall quality of generated molecules. The cosine distances between the fragment frequencies of the generated and reference set of molecules is known as Fragment similarity (Frag) where as Nearest neighbor similarity (SNN) denotes the average similarity of generated molecules to the nearest molecule from the reference set. The pairwise similarity of the generated molecules is denoted via Internal diversity (IntDiv). To measure the diversity, chemical and biological similarity of generated molecules, we used Fréchet ChemNet Distance (FCD)(Preuer et al., 2018) which uses last layer activation's of ChemNet to measure the differences. These metrics are evaluated on ZINC250K and QM9 dataset as reference set and results are shown in Table 9 and 10

Table 9: Evaluation of performance on MOSES metrics on generative models on QM9 dataset. FCD is lower the better, Frag, SNN, and IntDiv higher the better.

Method	FCD (↓)	Frag (↑)	SNN (↑)	IntDiv (↑)
GVAE	0.513	0.821	0.582	0.822
GraphEBM	0.551	0.831	0.547	0.831
GraphAF	0.732	0.863	0.565	0.823
GraphDF	0.683	0.892	0.562	0.839
MoFlow	0.496	0.840	0.502	0.852
`ModFlow` (2D-EGNN)	0.432	0.928	0.608	0.875
`ModFlow` (3D-EGNN)	0.478	0.934	0.613	0.885
`ModFlow` (JT-2D-EGNN)	0.421	0.921	0.595	0.867
`ModFlow` (JT-3D-EGNN)	0.401	0.939	0.624	0.889

Table 10: Evaluation of performance on MOSES metrics on generative models on ZINC250K dataset. FCD is lower the better, Frag, SNN, and IntDiv higher the better.

Method	FCD (↓)	Frag (↑)	SNN (↑)	IntDiv (↑)
JTVAE	0.512	0.890	0.5477	0.855
GVAE	0.571	0.871	0.532	0.852
GraphEBM	0.613	0.843	0.487	0.821
GraphAF	0.524	0.803	0.465	0.855
GraphDF	0.658	0.869	0.515	0.829
MoFlow	0.597	0.851	0.452	0.832
`ModFlow` (2D-EGNN)	0.495	0.891	0.570	0.863
`ModFlow` (3D-EGNN)	0.512	0.905	0.584	0.869
`ModFlow` (JT-2D-EGNN)	0.501	0.915	0.563	0.857
`ModFlow` (JT-3D-EGNN)	0.523	0.929	0.594	0.879

`ModFlow` achieves better performance results across all metrics. Notably, FCD score is low and IntDiv high, stating `ModFlow` is able to generate diverse set of molecules similar to what are present in dataset as compared to other methods.

Finally, we visually access the generated structures via properties distribution. We utilize kernel density estimation of these distributions to visualize these distributions. We use the following four properties:

- **Molecular weight (MW)**: the sum of the individual atomic weights of a molecule. The comparison will provide insight of generated molecule biasness toward lighter or heavier molecules.
- **LogP**: ratio of concentration in octanol-phase to aqueous phase, also known as the octanol-water partition coefficient. It is computed via Crippen (Wildman and Crippen, 1999) estimation.
- **Synthetic Accessibility Score (SA)**: an estimate describing the synthesizability of a given molecule. It is calculated using molecule's fragments contribution Ertl and Schuffenhauer (2009). .
- **Quantitative Estimation of Drug-likeness (QED)**: a value describing likeliness of a molecule as a viable candidate for a drug. It ranges between [0,1] and capture the abstract notion of esthetics in medicinal chemistry (Bickerton et al., 2012).

Fig. 7 and 8 shows the properties distribution between the generated molecules and the reference dataset. Notably, `ModFlow` matches the properties distribution very well, with some dispersion in QED and logP, demonstrating the effectiveness of the method in generating similar property molecules.

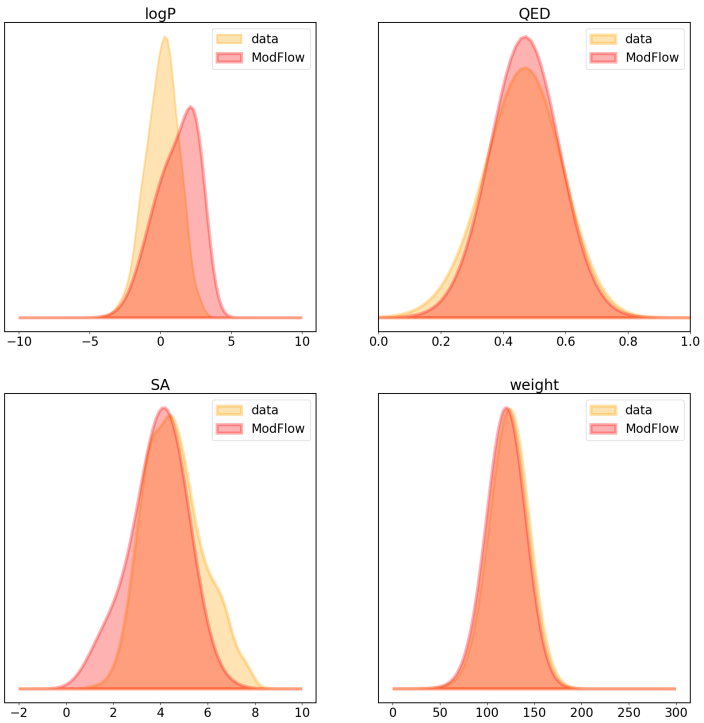

Figure 7: Distribution of chemical properties (quantitative estimation of drug-likeness (QED), molecular weight, synthetic accessibility score (SA), octanol-water partition coefficient (logP)) for the QM9 dataset and the set of generated molecules by `ModFlow`

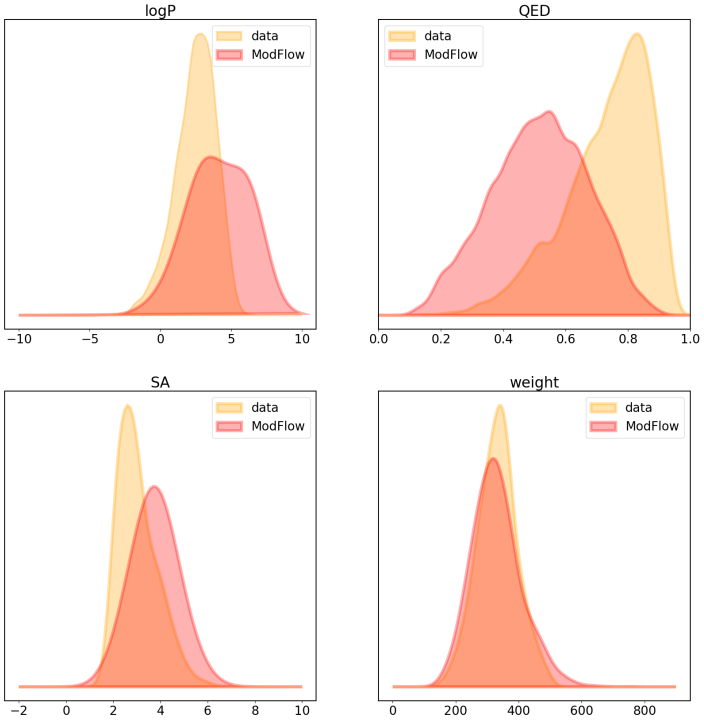

Figure 8: Distribution of chemical properties (quantitative estimation of drug-likeness (QED), molecular weight, synthetic accessibility score (SA), octanol-water partition coefficient (logP)) for the ZINC250k dataset and the set of generated molecules by `ModFlow`

A.7 Property-targeted Molecular Optimization

The task of molecular optimization is to search for the molecules, having a better chemical property. Specifically, we choose quantitative estimate of drug-likeness (QED) as our target chemical property. QED measures the potential of a molecule to be characterized as a drug. We used a pre-trained ModFlow model f, to encode a molecule $\mathcal{M}$ and get the embedding $Z = f(\mathcal{M})$, and further use linear regression to regress these embeddings to the QED scores of each molecule as our target chemical property. To discover new molecules, we interpolate in latent space of a molecule along the direction of increasing QED, via gradient ascend method, $Z' = Z + \lambda * \frac{dy}{dZ}$ where y is the QED score and λ is the length of the search step. The above method is conducting for K steps, and the new embedding Z' is decoded back to molecule space via reverse mapping $\mathcal{M}' = f^{-1}(Z')$.

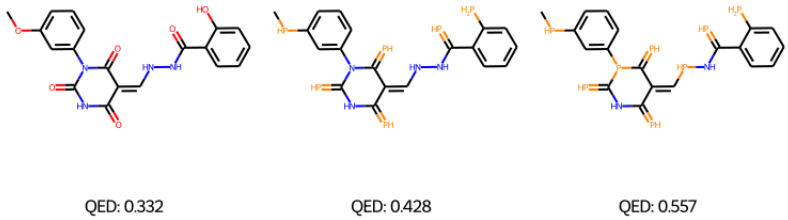

Figure 9: Chemical property optimization for ZINC250K dataset. Given the left-most molecule, we interpolate in latent space along the direction which maximizes its QED property.

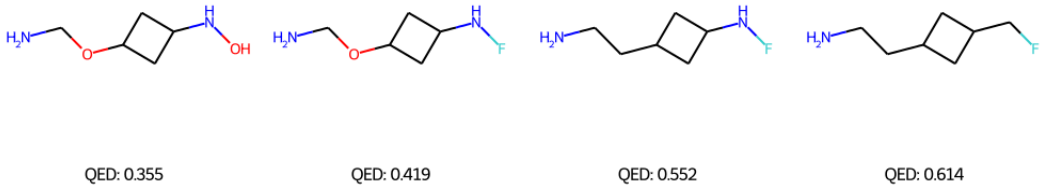

Figure 10: Chemical property optimization for QM9 dataset. Given the left-most molecule, we interpolate in latent space along the direction which maximizes its QED property.

Figure 9 and 10 represents the molecules decoded from the learned latent space with linear regression for successful molecular optimization. Here, we select molecules with low QED score and interpolate its latent space neighbourhood along the direction of increasing QED and then decode back to molecule. However, the number of valid molecules decoded back varies on the query molecule. We also report the discovered novel molecules sorted by their QED scores in Table 11 . We can see that `ModFlow` is able to find novel molecules with high QED score.

Table 11: Property optimization performance evaluated by best QED scores. Baselines are taken from Luo et al. (2021).

Method	1st	2nd	3rd
ZINC (dataset)	0.948	0.948	0.948
JTVAE	0.925	0.911	0.910
GCPN	0.948	0.947	0.945
MRNN	0.844	0.799	0.736
GraphAF	0.948	0.948	0.947
GraphDF	0.948	0.948	0.948
MoFlow	0.948	0.948	0.948
`ModFlow` (2D-EGNN)	0.948	0.941	0.937
`ModFlow` (3D-EGNN)	0.948	0.937	0.931
`ModFlow` (JT-2D-EGNN)	0.947	0.941	0.939
`ModFlow` (JT-3D-EGNN)	0.948	0.948	0.945
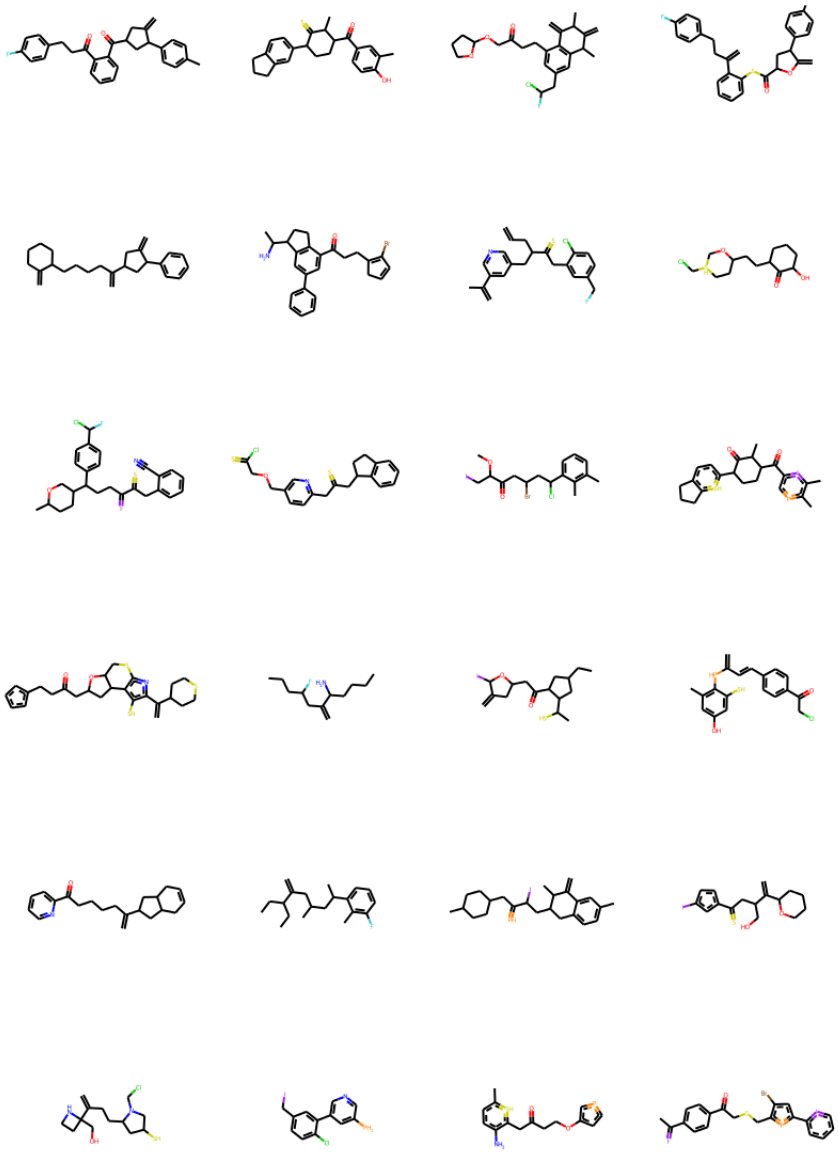
A.8 Additional examples of molecules generated by `ModFlow` .